

# Supporting Information for

## An integrally skinned asymmetric architecture design for advanced anion exchange membranes in vanadium flow batteries

Daishuang Zhang,<sup>a</sup> Xiaoming Yan,<sup>b</sup> Gaohong He,<sup>\*a</sup> Le Zhang,<sup>a</sup> Xinhong Liu,<sup>a</sup> Fengxiang Zhang,<sup>b</sup> Mengmeng Hu,<sup>a</sup> Yan Dai<sup>a</sup> and Sangshan Peng<sup>a</sup>

<sup>a</sup> State Key Laboratory of Fine Chemicals, Research and Development Center of Membrane Science and Technology, School of Chemical Engineering, Dalian University of Technology, Dalian, LN 116024, China.

<sup>b</sup> School of Petroleum and Chemical Engineering, Dalian University of Technology, Panjin, LN 124221, China.

E-mail: [hgaohong@dlut.edu.cn](mailto:hgaohong@dlut.edu.cn); Tel.: +86 411 84986291; Fax: +86 411 84986291.

### Experimental Procedures

#### 1. Membrane fabrication

**1.1 Synthesis of chloromethylated polysulfone (CMPSf-DC40/58%):** 20.0 g Polysulfone (P3500, Solvay Advanced Polymers, L.L.C., USA) was dissolved in 380 g dichloromethane (DAMAO, AR) in a 500 ml three-neck flask at room temperature, after the polymer was completely dissolved, the mixture was heated to 35 °C. Subsequently, 80 ml of chloromethyl octylether<sup>1</sup> and 2 ml of stannic chloride (Sinopharm Chemical Reagent Co. Ltd) were added. The reaction was kept in the flask equipped with a reflux condenser and a magnetic stirrer at 35 °C for a certain length of time (*i.e.*, 40 and 75 min). The resulting chloromethylated polysulfone (CMPSf) was obtained by pouring the reaction mixture into ethanol (DAMAO, AR), followed by thorough washing with ethanol. The CMPSf was dried overnight under vacuum at 40 °C prior to use. The CMPSfs (Scheme S2) synthesized had degrees of chloromethylation (DCs) of 40% and 58%, corresponding to the reaction time of 40 and 75 min, respectively. DC is defined as the average numbers of chloromethyl group attached to one PSf repeat unit in CMPSf.

**1.2 <sup>1</sup>H NMR spectroscopy:** <sup>1</sup>H NMR spectra were recorded on a Ascend™ 500 spectrometer at a resonance frequency of 500 MHz. Diluted CMPSf solutions were formed in deuterated chloroform, and tetramethylsilane was used as an internal standard. Based on <sup>1</sup>H NMR spectra of CMPSfs, the DC of CMPSf was estimated using the following equation:<sup>1</sup>

$$\text{DC} = \frac{2A(H_f)}{A(H_d)} \times 100\% \quad (\text{S1})$$

Where, A(H<sub>f</sub>) and A(H<sub>d</sub>) are the integral area of H<sub>f</sub> (hydrogen atoms in -CH<sub>2</sub>Cl) and H<sub>d</sub> (four hydrogen atoms adjacent to sulfone group in the aromatic ring) in the spectrum of CMPSf. For convenience, CMPSf with x% DC is denoted as CMPSf-DCx%.

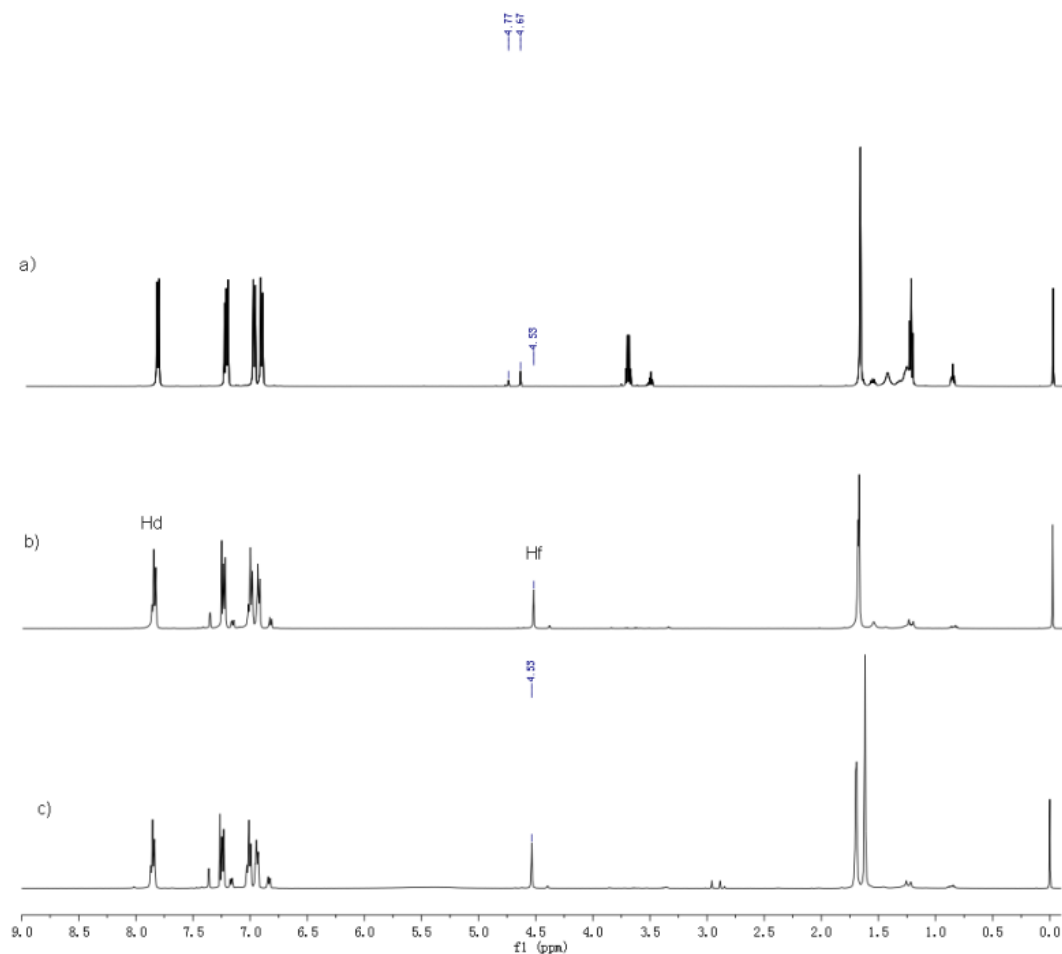


**Fig. S1**  $^1\text{H}$  NMR spectra of (a) polysulfone (PSf), (b) CMPSf-DC40%, and (c) CMPSf-DC58% in  $\text{CDCl}_3$ .

**1.3 Preparation of integrally skinned asymmetric anion exchange membranes (ISAAEMs) and dense AEMs:** Firstly, ISA CMPSf membranes (in the flat-sheet form) were made using the so-called dual-bath coagulation method,<sup>2</sup> which is illustrated in Scheme S3. The polymer solution (20 wt% CMPSf in 1-methyl-2-pyrrolidone (NMP) (DAMAO, AR)) was made by adding the measured polymers into NMP, followed by mixing in a heated magnetic stirrer maintained at 40 °C. Once dissolved, the solution was kept stirring for additional 12 h and then kept undisturbed at room temperature for 1 d to degas the solution. To form a uniform dense skin layer, the polymer solution was cast onto a clean glass plate with a constrained thickness of 200  $\mu\text{m}$  and was quickly soaked in 1-pentanol (DAMAO, AR) for a pre-determined time (*i.e.*, 20 s in this work), followed by immersing in deionized (DI) water for 24 h. The experiments in this study were performed during the autumn, winter, and early spring months, when water content in the air is low. Secondly, the ISA CMPSf membranes made herein were immersed in the 33 wt% trimethylamine aqueous solution (Tianjin Guangfu Fine Chemical Research Institute, CP) at 40 °C for 3 d to convert chloromethyl groups into quaternary ammonium moieties (*i.e.*, quaternized polysulfone, abbreviated as QAPSF). The resulting ISAAEMs were thoroughly washed with DI water several times to remove excess trimethylamine. The membranes in the sulfate form were achieved by ion exchange between chloride form membranes and 1 M sodium sulfate (Bodi, AR) at room temperature for 2 d, followed by thorough rinsing and immersion in DI water to remove excess salt. The dense CMPSf membrane ( $\sim 30 \mu\text{m}$ ) was fabricated by conventional solution casting method (4 wt% CMPSf in NMP as the polymer solution) a leveled glass dish. The solvent was let to evaporate at 50 °C for 72 h to form a dense membrane. Identical subsequent procedures were employed to fabricate a dense QAPSF membrane. Note: asymmetric membranes can be prepared using immersion-precipitation technique. Liquid-liquid demixing process in polymer solutions during membrane formation may occur in two different mechanisms, defined as delayed demixing and instantaneous demixing. Delayed demixing is possible when the interaction between solvent and nonsolvent is poor. Examples of such combinations are N-methylpyrrolidone (NMP), dimethylformamide (DMF) or N,N-dimethylacetamide (DMAc) as solvent and higher alcohols (e.g., propanol, butanol or pentanol) as nonsolvent. Instantaneous demixing proceeds if the interaction between solvent and nonsolvent is good. Combinations are NMP, DMF or DMAc as solvent and water as nonsolvent. It is favourable to have a combination of both mechanisms: an increase of the polymer concentration over a short period during the delayed demixing to obtain a dense skin layer, followed by the

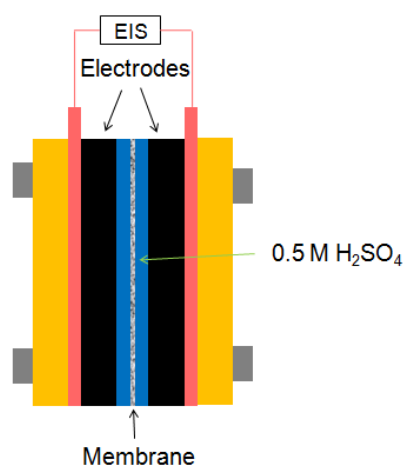
instantaneous demixing to get an interconnected sublayer. Chloromethylated polysulfone (CMPSf), the chosen polymer for membrane formation, was synthesized by the method mentioned above. NMP was used as the solvent for the dope formulation due to its strong interaction with CMPSf, and low levels of toxicity. 1-pentanol was selected as the first nonsolvent bath to enable the delayed demixing for the formation of a dense skin layer, and water as the second nonsolvent bath to obtain a well interconnected sublayer.

**1.4 The reference membranes:** fumasep®FAP-450 was supplied by FuMA-Tech GmbH (Germany), Nafion 212 was provided by DuPont (USA).

## 2. Membrane characterizations

**2.1 Membrane area resistance (AR):** The AR of the membranes was evaluated using conductivity cells with the method proposed elsewhere.<sup>3</sup> A conductivity cell composes of two half cells filled with 0.5 M H<sub>2</sub>SO<sub>4</sub> (Scheme S1). The effective area (S) of the cell is 3.2 cm<sup>2</sup>.  $r_1$  and  $r_2$ , which denote the electric resistance of the cell with and without a membrane, respectively, were measured by electrochemical impedance spectroscopy (Ivium Technologies, The Netherlands) over a frequency range from 1 MHz to 0.1 Hz. The AR of the membranes is determined by multiplying the membrane resistance and the effective area using the following equation:

$$AR = (r_1 - r_2) \times S \quad (S2)$$



**Scheme S1** The conductivity cell for evaluating membrane AR.

**2.2 Vanadium permeability:** The permeability of VO<sup>2+</sup> through the membranes was determined according to reported approach.<sup>4</sup> The left reservoir was filled with 50 ml of 1.5 M VOSO<sub>4</sub> in 3 M H<sub>2</sub>SO<sub>4</sub> solution and the right one was filled with 50 ml of 1.5 M MgSO<sub>4</sub> in 3 M H<sub>2</sub>SO<sub>4</sub> solution to equalize the ionic strengths and minimize the osmotic pressure effects. Magnetic stirrers were adopted in both reservoirs to mitigate concentration polarization. Samples from the right reservoir were withdrawn at regular time intervals (*i.e.*, 12 h). The absorbance of the sample solution was measured at a wavelength of 762 nm with a ultraviolet/Visible spectrophotometer (PERSEE, China) and was used to calculate the concentration of VO<sup>2+</sup> with regard to a readily plotted calibration curve. The VO<sup>2+</sup> permeability is calculated by using the following equation:

$$P = \frac{V_B L}{C_A A} \frac{dC_B(t)}{dt} \quad (S3)$$

in which  $V_B$  is the solution volume in the right reservoir (50 ml),  $A$  and  $L$  are the effective area and thickness of the membrane, respectively,  $P$  is the VO<sup>2+</sup> permeability of the membrane,  $C_A$  is the VO<sup>2+</sup> concentration in the left reservoir (1.5 M),  $C_B(t)$  is the concentration as a function of time in the right reservoir,  $dC_B/dt$  is the change of the VO<sup>2+</sup> concentration over time.

**2.3 The determination of IEC:** The ion exchange capacity (IEC, meq g<sup>-1</sup>) of each membrane used in this study was determined by acid-base titration method. The samples were soaked in 1 M NaOH solution at room temperature for 2 d to fully undergo ion exchange, during which chloride ions were substituted by hydroxide ions. The residual NaOH must be removed from the QAPSf membranes in the hydroxide form (QAPSfOH) before IEC characterization. During the NaOH elution, the QAPSfOH membranes were soaked in a DI H<sub>2</sub>O bath for 2-3 d, with daily renewal of the bath content with fresh DI water, until the pH of the rinsed DI water bath reached about 7. The QAPSfOH membranes were soaked in 20 ml of 0.01 M HCl at room temperature for 2 d, followed by titrating using 0.01 M NaOH with phenolphthalein as the indicator. The 20 ml of 0.01 M HCl was used as the blank sample. The IEC of the samples is calculated by:

$$IEC = \frac{(V_b - V_s) \cdot C_{NaOH}}{W_{dry}} \quad (S4)$$

Where  $V_b$  and  $V_s$  are the volume of NaOH solution consumed in the titration without and with membranes, respectively,  $C_{NaOH}$  is the mole concentration of NaOH solution, and  $W_{dry}$  is the mass of the dry membrane in the chloride form. Three replicates were manufactured for each sample.

**2.4 Mechanical strength:** A tensile tester (CMT8502, Shenzhen SANS Testing Machine Co. Ltd, China) was employed to probe the tensile stress-strain characteristics of fully hydrated QAPSF membranes in sulfate form at room temperature. A constant tensile speed of 10 mm min<sup>-1</sup> was adopted for sample measurements, all samples were prepared with a width of 5 mm and a length of 30 mm.

**2.5 Swelling degree:** Swelling degree is denoted as S.d.% in this work. The dimensions of the fully hydrated membranes (in sulfate form, denoted as  $X_{hyd}$ ) were recorded, and subsequently the membranes were dried in a vacuum oven at 60 °C for 24 h. Afterwards the dimensions,  $X_{dry}$ , of the dry membranes were collected again.

$$S.d.\% = \frac{X_{hyd} - X_{dry}}{X_{dry}} \times 100\% \quad (S5)$$

Where  $X_{hyd}$  and  $X_{dry}$  are the average dimension ( $X_{hyd} = (X_{hyd1} X_{hyd2})^{1/2}$ ,  $X_{dry} = (X_{dry1} X_{dry2})^{1/2}$ ) of the hydrated and dry membranes, respectively, in which  $X_{hyd1}$ ,  $X_{hyd2}$  and  $X_{dry1}$ ,  $X_{dry2}$  are the lengths and widths of the hydrated and dry membranes, respectively.

**2.6 Thermal stability:** Thermogravimetric analysis (TGA) was performed using a TGA Q50 (TA Instruments, USA). Each time, approximately 5 mg well-dried membrane sample was accurately weighed before being calcinated under high-purity N<sub>2</sub> flowing in the in-built Pt pan of the TGA instrument. The samples were programmed to be heated from room temperature to 600 °C at a heating rate of 10 °C min<sup>-1</sup>.

**2.7 Transmission electron microscopy:** Transmission electron microscopy (TEM) observations were performed on a transmission electron microscope (JEM-2000EX, JEOL, Japan) using an accelerating voltage of 120 kV. Prior to TEM observations, fully hydrated pristine QAPSF, fumasep®FAP-450 and Nafion 212 were first stained with PdCl<sub>4</sub><sup>2-</sup> and Pb<sup>2+</sup> by immersing in 0.01 M PdCl<sub>2</sub>/1 M HCl and 0.5 M lead nitrate aqueous solution, respectively, for 48 h. Then the stained samples were soaked in DI water to remove excess ions, followed by drying in a vacuum oven at 60 °C for 12 h.

**2.8 Scanning electron microscopy (SEM) characterization:** The cross-section SEM images were recorded on a Quanta 450 (FEI Co., USA). To eliminate charging effects during observation, the specimens were vacuum sputtered with gold for 90 s prior to characterization.

**2.9 The CO<sub>2</sub>/N<sub>2</sub> separation factor of ISAAEM:** The CO<sub>2</sub>/N<sub>2</sub> separation factor ( $\alpha$  (CO<sub>2</sub>/N<sub>2</sub>)) of DC40%-20s was measured using the time-lag method at 15 °C.<sup>5</sup> We shall consider permeability coefficients  $P_i$  and ideal separation factors for gas pairs CO<sub>2</sub> and N<sub>2</sub> defined as the ratio  $P(CO_2)/P(N_2)$ .  $P_i = Q_i L / A \Delta P$ , where  $Q_i$  is the gas flux,  $L$  is the membrane thickness,  $A$  is the membrane area, and  $\Delta P$  is the pressure differential.

### 3. Electrochemical measurements

**3.1 Cell construction:** Electrochemical performance of flow cells assembled with different membranes was evaluated using an in-house machined flow battery system. The system consisted of one single battery, two magnetic pumps (MP-10RN, Shanghai Xinxishan Industrial Co. Ltd, China), two glass reservoirs, and poly(tetrafluoro ethylene) tubing. The VFB single cell was constructed by sandwiching a separator between two carbon felt electrodes, clamped by two graphite current collectors. The depth of electrode cavity was 4 mm while the raw carbon felt electrodes had a nominal thickness of 5 mm, thusly a 20% compression rate was expected when the flow battery was sealed with fluorosilicon rubber gaskets. The carbon felt electrode (Gansu Hongwei Carbon Ltd, China) was oxidized in an air atmosphere at 400 °C for 6 h to improve electrochemical activity and hydrophilicity.<sup>6</sup> The effective transection area of the electrode and the separator was approximately 9 cm<sup>2</sup>.

**3.2 Electrolyte system:** A CT2001A battery tester (5V/1A) (LANHE, China) was employed to evaluate the performance of flow batteries and to control charging/discharging process of the electrolytes. The electrolyte flow rate to each half-cell was 40 ml min<sup>-1</sup>, which was provided by the magnetic pump. The starting electrolyte, 1.5 M VOSO<sub>4</sub> + 3.0 M H<sub>2</sub>SO<sub>4</sub>, was prepared by dissolving VOSO<sub>4</sub> 3.2 H<sub>2</sub>O (Shenyangshi Haizhongtian Fine Chemical Factory, 99% purity, China) in sulfuric acid. Anolyte and catholyte were prepared by charging the starting electrolyte to 1.65 V at 30 mA cm<sup>-2</sup> employing the normal flow cell unites, where 100 and 50 ml of the starting electrolyte were used for the positive and negative half-cells, respectively. After the charging voltage reached 1.65 V and potentiostatical charging at a constant potential of 1.65 V was carried out until the current density was below 5 mA cm<sup>-2</sup>. After that 50 ml of the formerly charged positive electrolyte was removed. Subsequently, the discharge voltage reached 0.8 V during discharging, demonstrating successful generation of ca. 50 ml anolyte (1.5 M VO<sup>2+</sup> in 4.5 M total sulfate) and ca. 50 ml catholyte (1.5 M V<sup>3+</sup> in 4.5 M total sulfate) through electrochemical oxidation and reduction of 1.5 M VOSO<sub>4</sub> in 4.5 M total sulfate.

**3.3 Single cell electrochemical performance evaluation:** The electrochemical performance of flow cells assembled with various membranes was tested by using a CT2001A potentiostat/galvanostat station (LANHE,

China). For cell performance evaluation, the battery was charged to a maximum potential of 1.65 V and then discharged to a minimum potential of 0.80 V with current densities from 20 to 100 mA cm<sup>-2</sup>. Cell cycling tests were carried out at a constant charging/discharging current density of 50 mA cm<sup>-2</sup>. Two reservoirs were initially purged with nitrogen and then sealed by valves. The nitrogen purged in the negative electrolyte reservoir was used to prevent the highly reducing V<sup>2+</sup> from being oxidized into V<sup>3+</sup>. A water bath was used to control the temperature of electrolytes during flow battery tests.

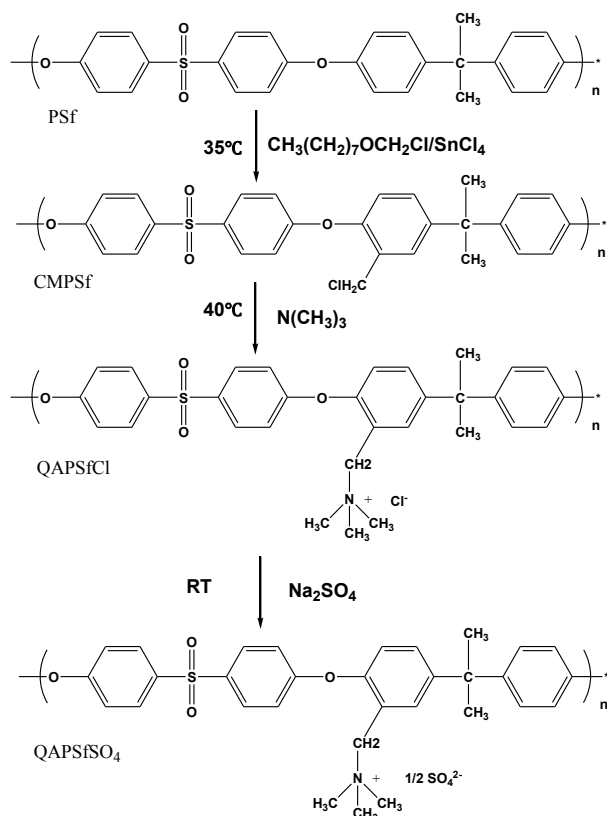
Efficiencies are defined as:

$$\text{Coulombic efficiency (CE)} = \int i_d dt / \int i_c dt$$

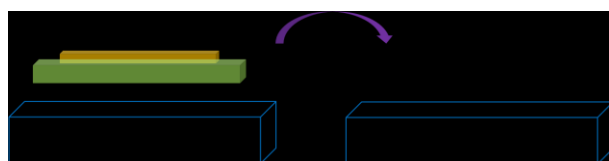
$$\text{Energy efficiency (EE)} = \int V_d i_d dt / \int V_c i_c dt$$

$$\text{Voltage efficiency (VE)} = \text{EE/CE}$$

where *i* represents current, *V* denotes voltage, and subscripts of *c* and *d* are charging and discharging, respectively.



**Scheme S2** The synthetic procedure of QAPSF with sulfate anions.



**Scheme S3** Schematic of the experimental process for fabricating integrally skinned asymmetric CMPSf membranes.

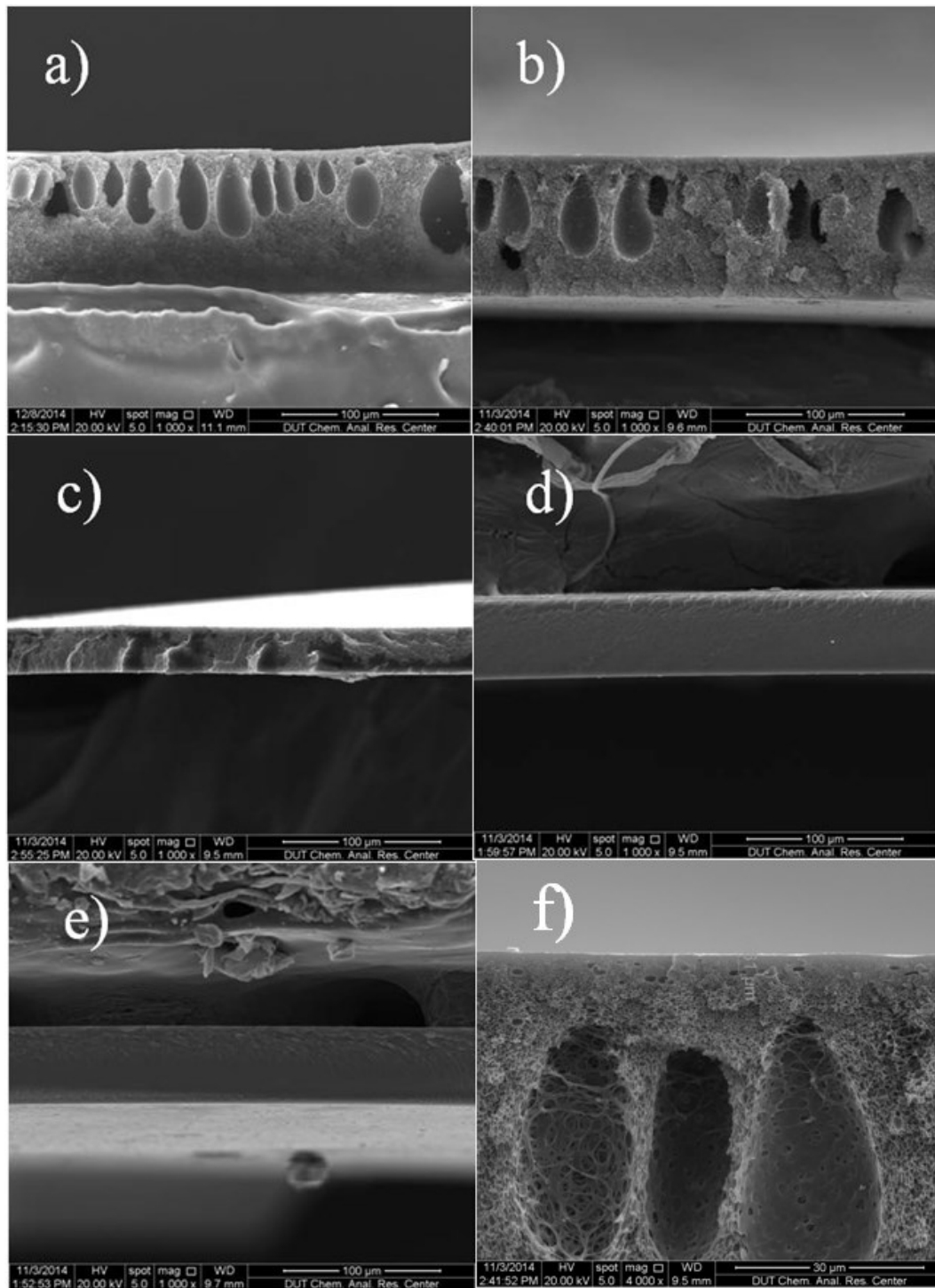


**Fig. S2** Low-resolution SEM images of (a) DC40%-20s, (b) DC58%-20s, (c) Dense DC40%, (d) fumasep@FAP-450, and (e) Nafion 212. And (f) high-magnification SEM image of DC58%-20s. (a-e) all scale bars are 100 μm, (f) scale bar is 30 μm.

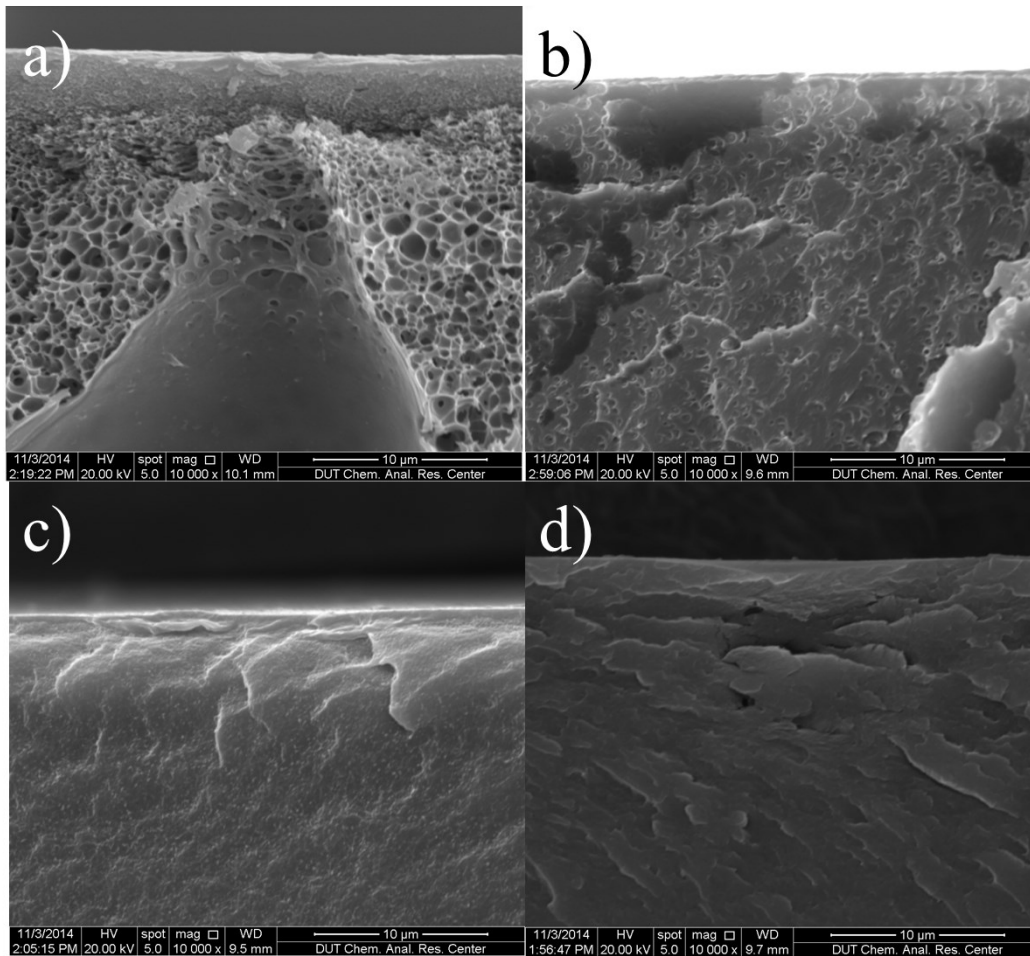


**Fig. S3** High-resolution cross-section SEM images of (a) DC40%-20s, (b) Dense DC40%, (c) fumasep®FAP-450, and (d) Nafion 212. All scale bars are 10 µm.

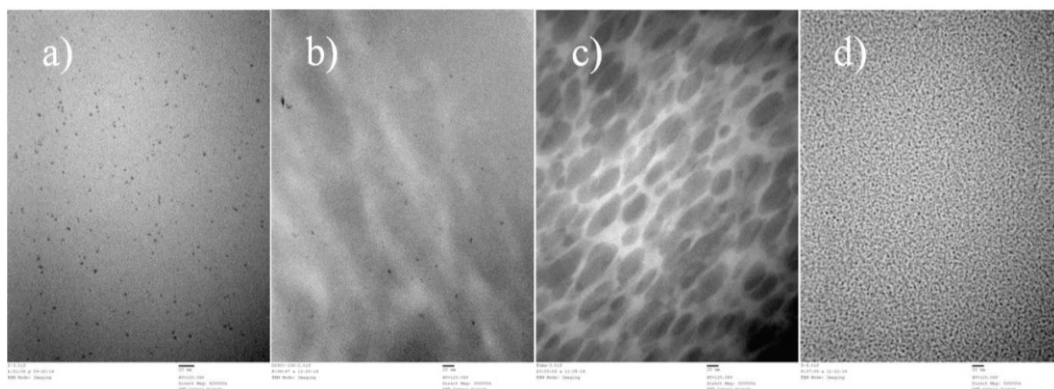


**Fig. S4** TEM images of (a) DC58%-20s, (b) DC40%-20s, (c) fumasep®FAP-450, and (d) Nafion 212. All scale bars are 20 nm.

From TEM images, as shown in Fig. S4, the ion pairs of ionomers have been shown to aggregate into domains of high ion content (dark regions), which are surrounded by domains of low ion content (light regions). The size of the ionic clusters was found to increase with increasing IEC; meanwhile, average separation distance between the ionic clusters decreased with increasing IEC (shown in Fig. S4a and b). Interestingly, the ionic clusters of fumasep®FAP-450 are clearly much larger in size than that of other ion exchange membranes (IEMs) (*e.g.*, DC58%-20s, DC40%-20s, Nafion 212), which would account for the observed relatively rapid decay in discharge capacity for fumasep®FAP-450 membrane (see Fig. S9a). Furthermore, the ionic clusters of fumasep®FAP-450 are oriented, nearly ellipsoidal in shape distinctly different from that of the other IEMs, which are spherical. In the case of Nafion 212, the ionic cluster diameter is approximately less than 5 nm, consistent with the value proposed by Schmidt-Rohr's model.<sup>7</sup>

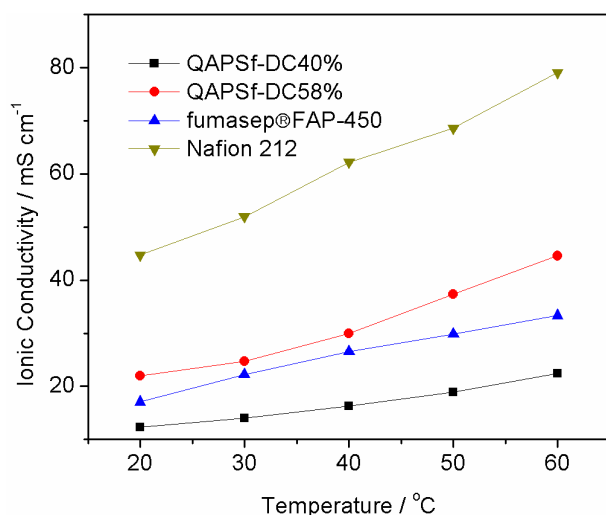


**Fig. S5** Temperature-dependent ionic conductivity.

The polymer precursors for QAPSF-DC40% and QAPSF-DC58% (dense membranes) are CMPSfs with DCs of 40% and 58%, respectively.



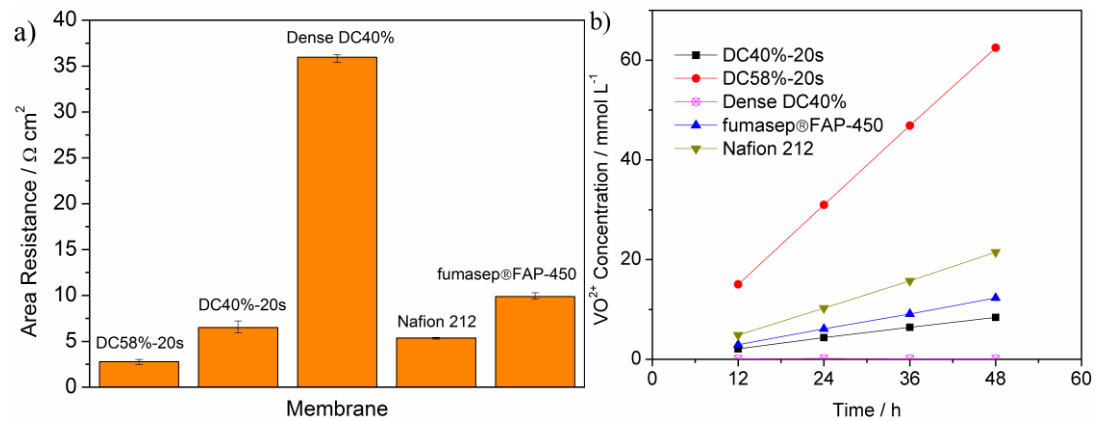


**Fig. S6** (a) Area resistance of as-fabricated membranes and commercially available membranes. (b) Vanadium diffusion across as-fabricated and commercially available membranes.

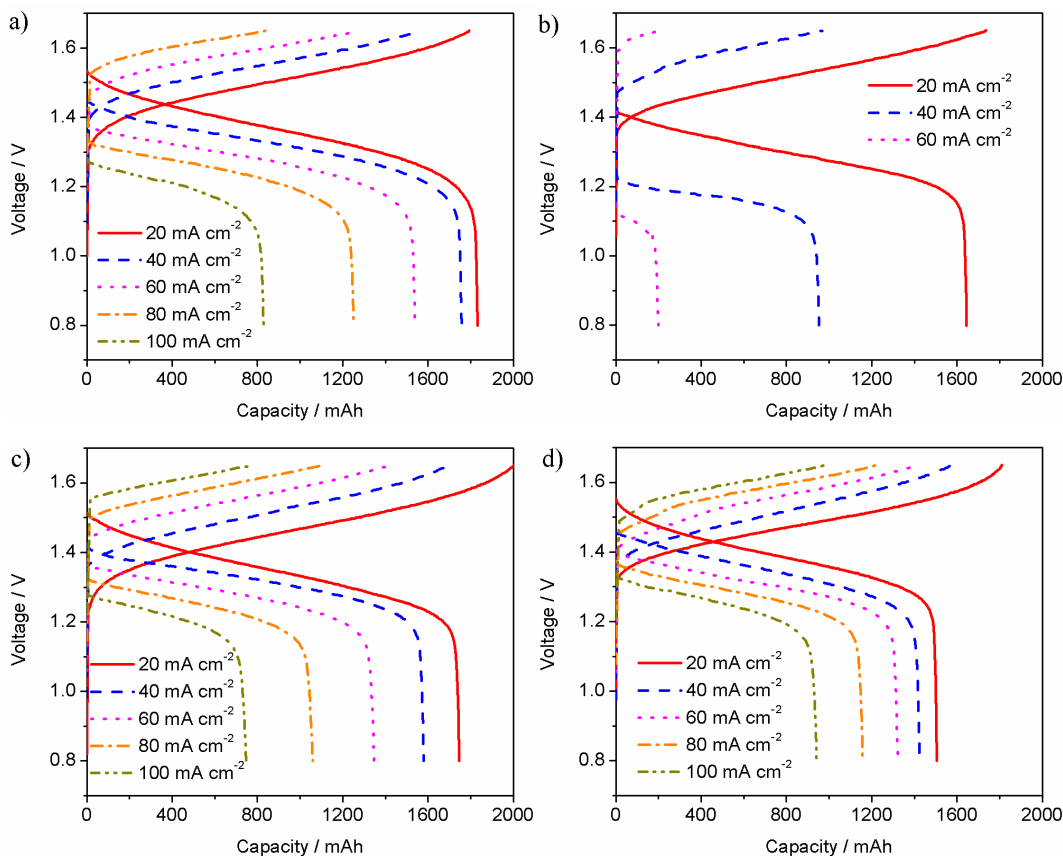


**Fig. S7** Charge-discharge voltage profiles of (a) DC40%-20s, (b) Dense DC40%, (c) fumasep®FAP-450, and (d) Nafion 212. Nafion 212 and fumasep®FAP-450 were used as references. All tests were performed under the identical operating mode.

The electrochemical performances of the as-fabricated membranes and commercially available membranes (*i.e.*, Nafion 212 and fumasep®FAP-450) in VFB single cells were evaluated employing the identical single cell and test environments. As displayed in Figs. S6 and S7f, the charge/discharge capacities of VFB single cells assembled with all of the separators decreased with increasing current density, which can be ascribed to the increase of the polarization, which mainly includes membrane ohmic loss and concentration polarization under specific current density. Furthermore, the charge/discharge capacities were apparently reduced following variant magnitudes, which could be principally attributed to the different ARs of the membranes. For example, in the case of DC40%-20s, the discharge capacities decreased by 55% from 1831 to 828 mAh as the current density increased from 20 to 100 mA cm<sup>-2</sup>, while in the case of Dense DC40%, witnessed an 88% shrinkage from 1645 to 198.2 mAh from 20 to 60 mA cm<sup>-2</sup>. The above results evidently demonstrate the advantage of ISAAEMs over dense AEMs with low IEC, especially at high current densities. As shown in Fig. S7b, the VFB single cell assembled with Dense DC40% cannot be charged under current densities ranging from 80 to 100 mA cm<sup>-2</sup> because of severe overpotential mainly resulted from the high AR of Dense DC40% (see Fig. S6a). Moreover, Nafion 212 was more advantageous in discharge capacity than other membranes under high current density of 100 mA cm<sup>-2</sup>, whereas other membranes delivered larger discharge capacity than Nafion 212 under low current density (*e.g.*, 20 mA cm<sup>-2</sup>).

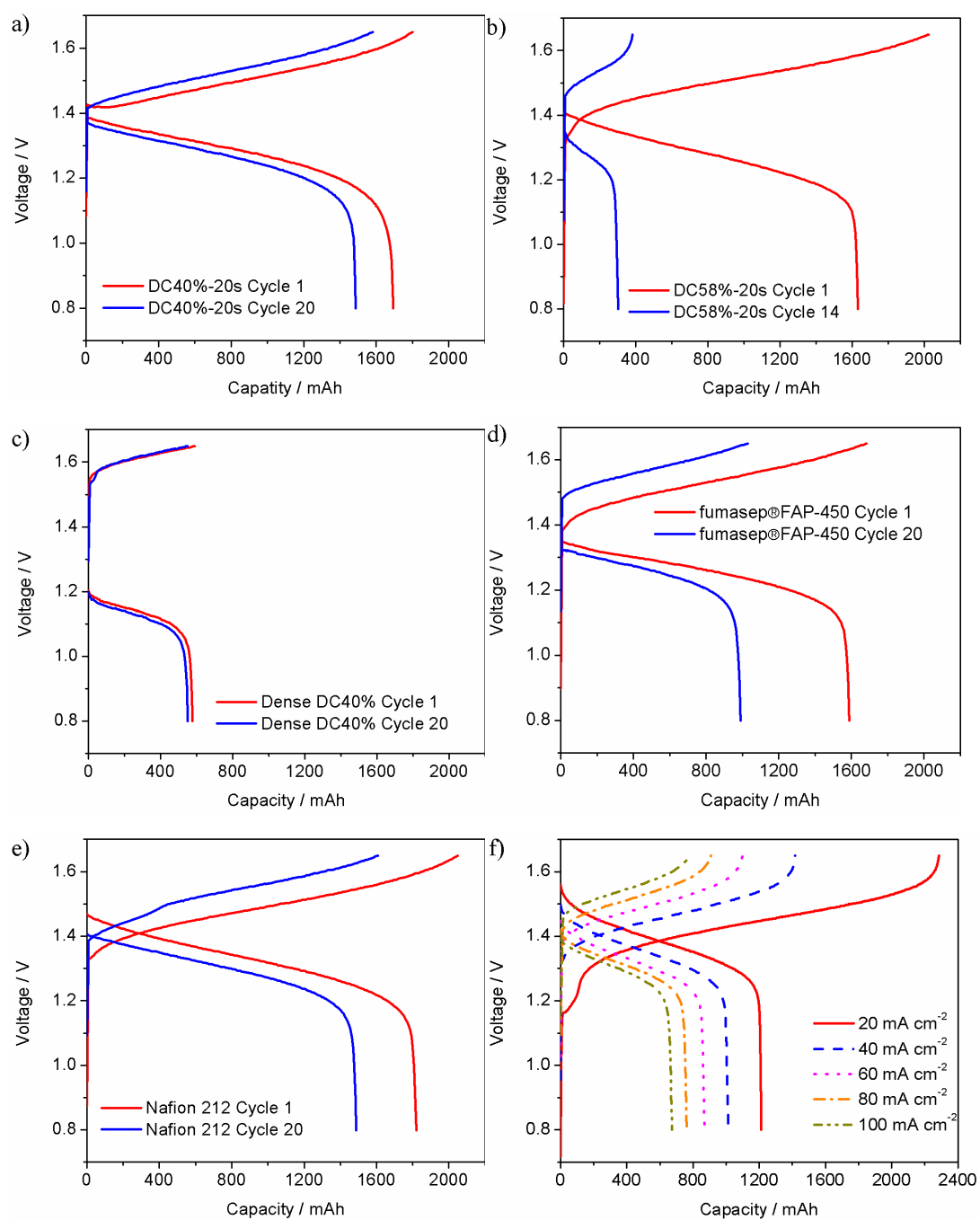


**Fig. S8** (a)-(e) Cell voltage profile with respect to cell capacity at different charge-discharge cycles and (f) charge-discharge voltage profiles of DC58%-20s at different current densities.

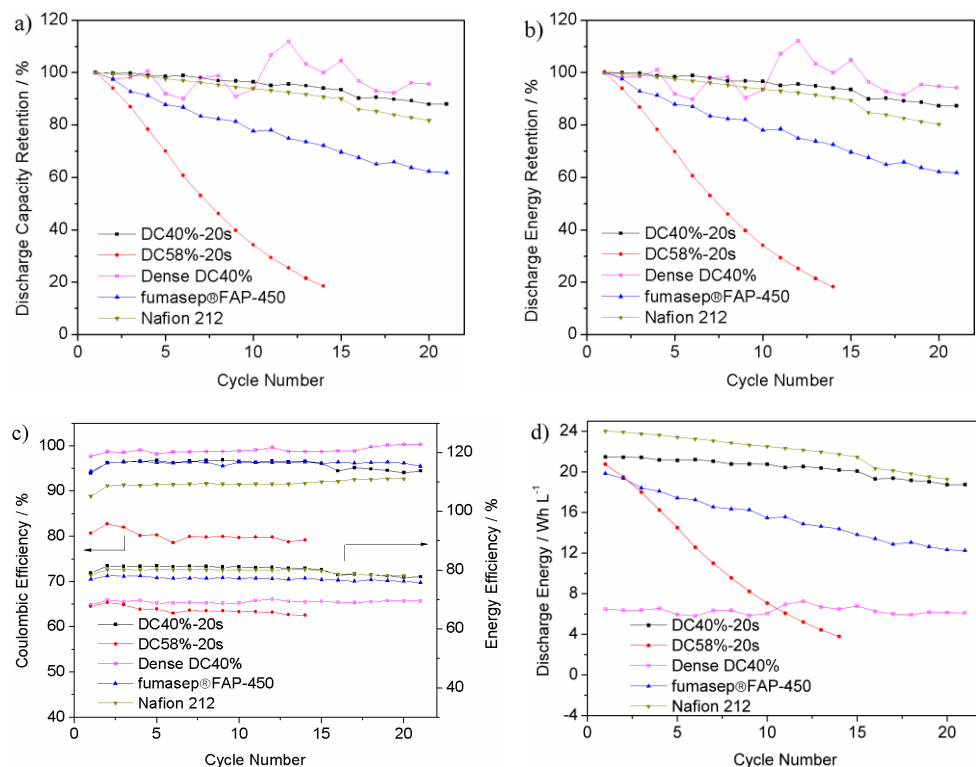


**Fig. S9** Electrochemical performance of VFBS employing different membranes over cycling at  $50 \text{ mA cm}^{-2}$ : (a) normalized discharge capacity over cycling, (b) normalized discharge energy over cycling, (c) CE and EE over cycling, and (d) discharge energy decay over cycling.

IEMs inevitably cause vanadium active species imbalance and asymmetrical valence of vanadium ions in positive and negative half-cells, these out-of-balance cell states are resulted from different permeation rates of four vanadium species and subsequent self-discharge reactions.<sup>4, 8-10</sup> Failing to maintain balance between active species of different valence would definitely lead to cell capacity fading. Better capacity retention ability implies less frequent need for electrolyte maintenances, which is the common remedy required to reinstate electrolyte balance, resulting in a reduction in operating cost.

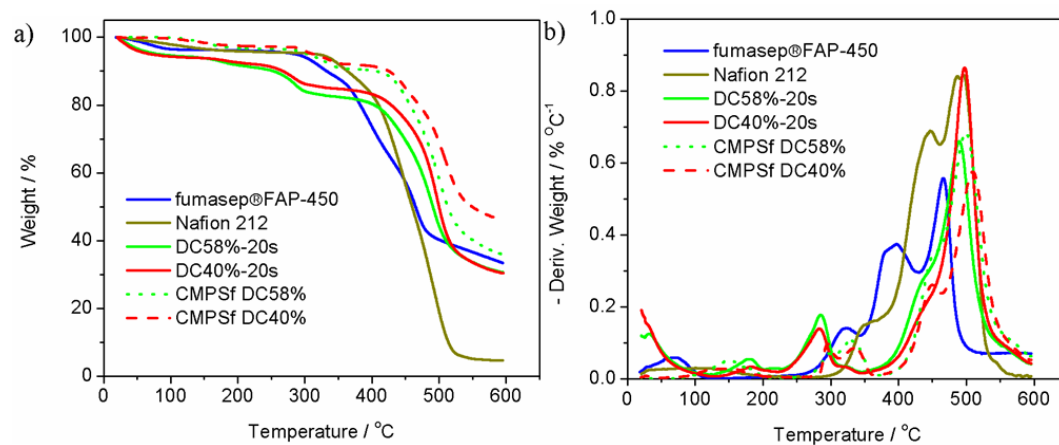


**Fig. S10** (a) Thermogravimetric analysis (TGA) curves; (b) differential TGA curves.

For DC40%-20s and DC58%-20s, a two-step thermal degradation profile was observed. The weight loss before  $200 \text{ }^\circ\text{C}$  is mainly due to the evaporation of free and bound waters. The weight loss at around  $280 \text{ }^\circ\text{C}$  is associated with the degradation of the quaternary ammonium groups. The apparent weight loss at around  $500 \text{ }^\circ\text{C}$  is related to the degradation of the polymer chain. DC40%-20s has better thermal stability than DC58%-20s, which can be attributed to smaller content of quaternary ammonium groups in DC40%-20s.

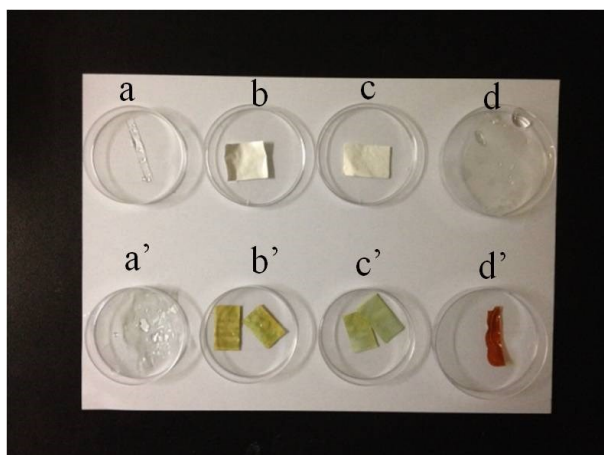


**Fig. S11** Accelerated chemical stability tests of DC40%-20s, DC58%-20s, fumasep®FAP-450, and Nafion 212. (a) Nafion 212, (b) DC58%-20s, (c) DC40%-20s, (d) fumasep®FAP-450 before test. (a') Nafion 212, (b') DC58%-20s, (c') DC40%-20s, (d') fumasep®FAP-450 after test.

The different membranes were immersed in 1.5 M  $\text{VO}_2^+$  + 3.0 M  $\text{H}_2\text{SO}_4$  electrolyte solutions at ambient temperature for 31 days. All the membranes remained intact and flexible after soaking in 1.5 M  $\text{VO}_2^+$  + 3.0 M  $\text{H}_2\text{SO}_4$  electrolyte solution for 31 days, but the colors of all the membranes, except Nafion 212, had changed and became distinctly different, as shown in the above figure. The fumasep®FAP-450 membrane became dark red, whereas the DC40%-20s and DC58%-20s membranes became yellow/green. Moreover, the DC40%-20s membrane displayed lighter color than the DC58%-20s membrane, indicating better chemical stability.

Table S1. The mechanical properties.

Sample	Elongation at break	Maximum tensile strength	Swelling ratio
	(%)	(MPa)	(%)
DC40%-20s	80.21	5.54	6.39
DC58%-20s	66.7	2.95	9.48
Dense DC40%	34.80	27.86	Hardly observed
fumasep®FAP-450	579.96	17.47	4.34
Nafion 212	119.32	11.72	12.98

Table S2. The volume variations of the electrolytes at both positive and negative half-cells.

Sample	Positive half-cells		Negative half-cells	
	Electrolyte volume in the first cycle	Electrolyte volume after cycling	Electrolyte volume in the first cycle	Electrolyte volume after cycling
	(ml)	(ml)	(ml)	(ml)
DC40%-20s <sup>a</sup>	51.5	50.0	44.0	45.0
DC58%-20s <sup>b</sup>	53.8	31.7	47.5	68.9
Dense DC40% <sup>c</sup>	53.5	53.0	45.5	46.5
fumasep®FAP-450 <sup>d</sup>	53.5	47.0	46.6	51.0
Nafion 212 <sup>e</sup>	55.0	57.5	47.0	43.9

<sup>a</sup> Over 21 cycles, <sup>b</sup> Over 14 cycles, <sup>c</sup> Over 20 cycles, <sup>d</sup> Over 21 cycles, <sup>e</sup> Over 20 cycles.

The total volume of positive and negative electrolytes is constant over cycling. In reality, the discrepancy is due to the experimental error.

Table S3. Weight variations after the chemical stability tests.

Sample	IEC (meq g <sup>-1</sup> )	Weight before test <sup>c</sup> (g)	Weight after test <sup>d</sup> (g)	Weight variation (%)
DC40%-20s	0.72 <sup>a</sup>	0.0353	0.0351	-0.57
DC58%-20s	1.01 <sup>a</sup>	0.0361	0.0354	-1.94
fumasep®FAP-450	1.16 <sup>11</sup>	0.0344	0.0352	+2.33
Nafion 212	0.92 <sup>b</sup>	0.0526	0.0529	+0.57

<sup>a</sup> Ion exchange capacity (IEC) was measured by titration. <sup>b</sup> Provided by DuPont™. <sup>c</sup> Measured after thorough drying. <sup>d</sup> Measured after thorough washing and drying.

The DC40%-20s membrane with IEC of 0.72 meq g<sup>-1</sup> displayed much less weight variation than the DC58%-20s membrane with IEC of 1.01 meq g<sup>-1</sup>, suggesting membranes with lower IEC have better chemical stability than those with higher IEC. The increased weight of fumasep®FAP-450 and Nafion 212 after test may largely be attributed to the VO<sub>2</sub><sup>+</sup> ions absorbed into respective ionic clusters.<sup>12</sup>

## References

1. X. Yan, G. He, S. Gu, X. Wu, L. Du and Y. Wang, *International Journal of Hydrogen Energy*, 2012, **37**, 5216.
2. (a) J. A. van't Hof, A. J. Reuvers, R. M. Boom, H. H. M. Rolevink and C. A. Smolders, *Journal of Membrane Science*, 1992, **70**, 17; (b) S.-G. Li, G. H. Koops, M. H. V. Mulder, T. van den Boomgaard and C. A. Smolders, *Journal of Membrane Science*, 1994, **94**, 329; (c) G. H. Koops, J. A. M. Nolten, M. H. V. Mulder and C. A. Smolders, *Journal of Applied Polymer Science*, 1994, **54**, 385; (d) J. Kurdi and A. Y. Tremblay, *Journal of Applied Polymer Science*, 1999, **73**, 1471; (e) Q. Yang, T. S. Chung and Y. E. Santoso, *Journal of Membrane Science*, 2007, **290**, 153.
3. H. Zhang, H. Zhang, X. Li, Z. Mai and W. Wei, *Energy & Environmental Science*, 2012, **5**, 6299.
4. Q. Luo, L. Li, W. Wang, Z. Nie, X. Wei, B. Li, B. Chen, Z. Yang and V. Sprenkle, *ChemSusChem*, 2013, **6**, 268.
5. J. Ahn, W.-J. Chung, I. Pinnau and M. D. Guiver, *Journal of Membrane Science*, 2008, **314**, 123.
6. L. Li, S. Kim, W. Wang, M. Vijayakumar, Z. Nie, B. Chen, J. Zhang, G. Xia, J. Hu, G. Graff, J. Liu and Z. Yang, *Advanced Energy Materials*, 2011, **1**, 394.
7. K. Schmidt-Rohr and Q. Chen, *Nature Materials*, 2008, **7**, 75.
8. J. Sun, X. Li, X. Xi, Q. Lai, T. Liu and H. Zhang, *Journal of Power Sources*, 2014, **271**, 1.
9. C. Sun, J. Chen, H. Zhang, X. Han and Q. Luo, *Journal of Power Sources*, 2010, **195**, 890.
10. X. Wei, Z. Nie, Q. Luo, B. Li, B. Chen, K. Simmons, V. Sprenkle and W. Wang, *Advanced Energy Materials*, 2013, **3**, 1215.
11. P. K. Leung, Q. Xu, T. S. Zhao, L. Zeng and C. Zhang, *Electrochimica Acta*, 2013, **105**, 584.
12. H.-S. Cho, M. Ohashi and J. W. Van Zee, *Journal of Power Sources*, 2014, **267**, 547.